The tsunami signature on a submerged promontory: the case study of the Atacames Promontory, Ecuador

M. Ioualalen, Gueorgui Ratzov, J.-Y. Collot, E. Sanclemente

The tsunami signature on a submerged promontory: the case study of the Atacames Promontory, Ecuador

M. Ioualalen,[1] G. Ratzov,[1] J.-Y. Collot[1] and E. Sanclemente[2]

[1]*Institut de Recherche pour le Développement, IRD, GéoAzur (IRD - UNSA - CNRS - OCA), Villefranche-sur-mer, France.*
E-mail: Mansour.Ioualalen@geoazur.obs-vlfr.fr
[2]*Facultad de Ingenieria en Ciencias de la Tierra, FICT, (ESPOL), Guayaquil, Ecuador*

GJI Marine geosciences and applied geophysics

SUMMARY
Shelf promontories exhibit very specific bathymetric features with regards to tsunamis. Because of their submerged cape morphology, a potential tsunami generated seawards of the promontory will exhibit a specific mode of propagation and coastal impact. To identify this peculiar tsunami signature, the Atacames Promontory, Ecuador, was chosen as a case study (another example is the shelf of the Nile delta, Egypt). The area is tectonically very active, hosts earthquakes among the most powerful recorded, as well as areas of slope instabilities that have triggered significant submarine landslides in the past (several cubic kilometres of volume). Both types of events are likely to be tsunamigenic. To examine the tsunami behaviour at the coastal area of the promontory and at its vicinity, we have considered two examples of tsunamigenic landslides of which scars were identified near the base of the continental slope. We also took into consideration two earthquake scenarios that are likely to represent most classes of earthquakes possibly occurring in this area depending on their locations and subsequent tsunami directivity, that is, a sensitivity test investigation. We took two distinct earthquake scenarios which are based on the 1942 and 1958 events that stroke the area. Then we computed their derived tsunamis and analysed their coastal impact. We found that significant tsunamis can be generated by either landslides or earthquakes. However, the maxima of wave amplitude occur offshore (but still above the underwater promontory): the concave-type shape of the bathymetric field often yields a refraction/focusing area that is located on the shelf promontory and not at the coast area of the promontory: the wave propagates first through the focusing area before striking the considered coast. This area may be considered as a sheltered zone. Besides, in the vicinity of the promontory (not exactly concerned by the study), the city of Esmeraldas, is relatively sheltered due to the presence of the underwater canyon at its termination and due to diverging waves.

Key words: Tsunamis; Site effects; Wave propagation; Submarine landslides; South America.

1 INTRODUCTION

Shelf promontories, or submerged capes, present a peculiar bathymetric shape: the iso-levels of water depths, that is, the isobaths are generally concave shaped (the centre of the radius of curvature is located landward) so that shelf promontories should tend to host tsunami focusing areas. Consequently, the tsunami impact on the nearby coast should strongly depend on such submerged morphological features. In this work, we selected the shallow submerged Atacames Promontory in northern Ecuador (Fig. 1) to identify its effects on both the tsunami propagation and impact on the adjacent coastline. The region is located in a subduction zone, where tsunamigenic earthquakes are numerous (Kanamori & McNally 1982; Beck & Ruff 1984) and among the most powerful on the Earth. Another potential source of tsunamis is the presence of unstable seafloor sed-

imented slopes that may slide catastrophically in response to various triggers. Numerous morphologic scars of submarine mass failures (SMFs) were detected from high-resolution swath bathymetric data in the vicinity of the promontory (Collot *et al.* 2005; Ratzov *et al.* 2007). Several associated mass transport deposits were identified from 3.5 kHz seismic data, in the adjacent subduction trench (Ratzov *et al.* 2010), thus attesting of recurrent events. Beside their contribution to margin erosion and sediment transfers from the slope to the trench, SMFs present a non-negligeable natural risk. They may damage marine infrastructures or submerged communication cables, and generate tsunamis. The 1979 October 16 SMF(s) and associated tsunami in the French Riviera are examples of such natural risk: following a collapse of an extension of the Nice city harbour close to the international airport, submarine cables were destroyed and the SMF(s) killed 10 people working on the site while another
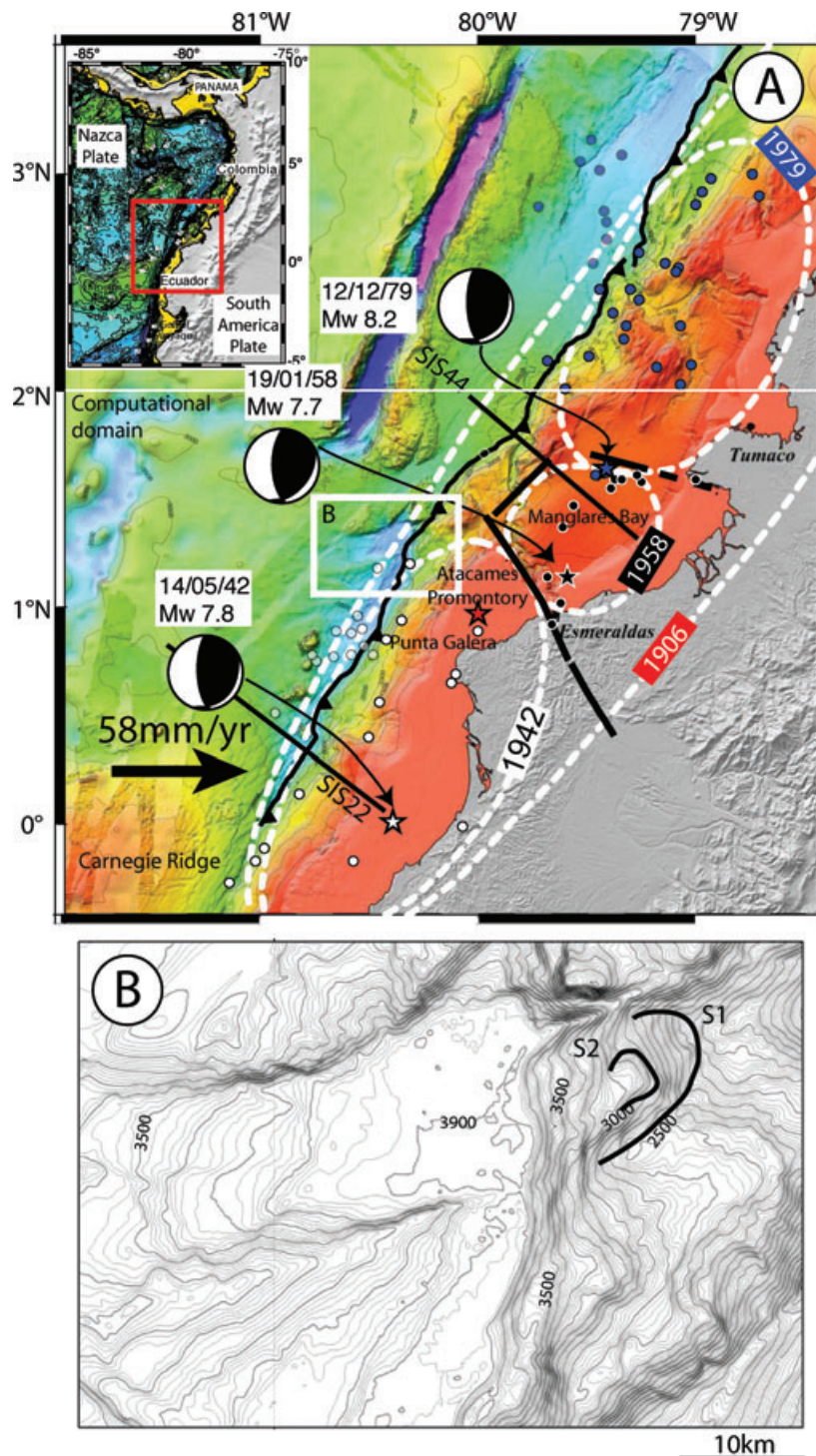
Figure 1. (A) Bathymetric map of the North Ecuador–South Colombia convergent margin as compiled by Michaud *et al.* (2006) from swath bathymetic data and satellite-derived bathymetry (Smith & Sandwell 1997) (500 m intervals). The bold dashed curve represents the northern limit of the Carnegie Ridge. The computational domain boundaries are represented. The barbed line is the deformation front along the trench. The black vector indicates plate convergence after Trenkamp *et al.* (2002). The ruptured zones are represented for the four major earthquakes of the last century: The 1906 January 31 (8.8 *M*w), the 1942 May 14 (7.9 *M*w) ; the 1958 January 19 (7.8 *M*w) and the 1979 December 12 (8.2 *M*w). The tracks for the two seismic profiles SIS44 and SIS22 gathered during the SISTEUR cruise are also represented. (B) The margin front (white rectangle B in panel A) is enlarged: 100 m (bold)—and 20 m— isobaths contours. S1 and S2 represent the SMFs scars limits.

victim was recorded few miles away, in Antibes city, due to the 2–3 m tsunami wave that had been generated (Assier-Rzadkiewicz *et al.* 2000; Ioualalen *et al.* 2010). The most recent and documented event is the SMF/slump that occurred offshore Papua New Guinea on 1998 July 17 (Tappin *et al.* 2008). The event caused the loss of over 2200 lives and naturally raised concerns about potential damaging effects of SMF-generated tsunamis. As a comparison, Ioualalen *et al.* (2010) identified scars of past landslides offshore

the Ligurian Sea (French Riviera) and found that volumes of 2–3 km³ could have generated tsunamis with wave amplitude in the order of 6–7 m, at some specific areas. We expect that landslides of several cubic kilometres evidenced in the North Ecuadorian/South Colombian margin (Ratzov *et al.* 2010) could have generated significant tsunamis.

To tentatively describe the tsunami signature in such coastal environment through sensitivity tests, we selected a wide range of tsunami sources in terms of wave directivity mainly, but also in terms of wave height, that are likely to describe the tsunami threat in the area. We used SMFs that are well identified by their bathymetric scars as potential tsunamigenic sources. Expanding our study to tsunamigenic earthquakes we considered the 1942 May 14 and the 1958 January 19 earthquakes that were located in the vicinity of the promontory.

2 MORPHOLOGY OF STUDY AREA: ORIGIN AND EVOLUTION OF THE ATACAMES PROMONTORY

The generally NNE-trending coastline of Ecuador bends sharply to 70°N trending, northeastward of Punta Galera, and exhibits >100 m-high cliffs, with the exception of notable alluvial plains that surround the Atacames and Esmeraldas cities, and extends locally upwards the river valleys (Fig. 1). Offshore Punta Galera and Atacames cities, the continental shelf is 60–120 m deep and extends broadly northwards over ∼45 km, thus forming the submerged, concave-shaped Atacames Promontory. The shelf narrows to ∼15 km eastwards, offshore the Esmeraldas city, where the shelf edge forms a smooth, convex-shaped re-entrant that reflects the morphology of the Manglares Bay. Both the Atacames Promontory and the wide shelf re-entrant facing Esmeraldas are crucial in terms of tsunami mode of amplification/attenuation. The submarine Esmeraldas canyon, which breaches the shelf and extends northwards from the Esmeraldas City, may also play a crucial role in tsunami propagation, for example, Ioualalen *et al.* (2007) showed how the multiple canyons of the Bangladesh shelf limited the impact of the 2004 Sumatra event on the coast of Bangladesh.

Westward of the Atacames Promontory, the margin slope is steep (∼ 9°) and deepens to ∼ 3900 m in the trench. It is gentler at water depths shallower than 1500 m (∼ 7°), and its N25° orientation, up to latitude 1°15′N (∼ 45 km NE of Punta Galera), rotates progressively eastwards to reach a N120° trend.

Although the Atacames Promontory is likely to condition the potential tsunami signature at the nearby coastal area, the notion of tsunami risk assessment that is commonly used, does not apply for geological timescales (from its origin to present including its evolution). It is however interesting to review the timescale estimates of the promontory dynamics and also to mention that the promontory has not always been submerged and, consequently, the tsunami signature may also evolve on a geological timescale. The evolution of the submerged Atacames promontory likely responds to long-term tectonic and short-term climatic factors. Based on morphological, geological and kinematic considerations, Collot *et al.* (2010) proposed that the Atacames Promontory resulted from the long-term uplift of the inner trench slope and coastal area, in relation with the subduction of the Carnegie Ridge. According to these authors, the ENE-trending northern flank of the Carnegie Ridge (Fig. 1) migrated southwards along the north Ecuador trench, so that a ridge segment, possibly offset by a NS-trending Panama basin Fracture Zones, would presently underlay the promontory. This interpretation

is substantiated by nearby onshore Pleistocene marine terraces that uplifted with a 0.32 mm yr⁻¹ rate since at least 220 kyr (Pedoja *et al.* 2006). Following this scheme, and in absence of clues for present day subsidence, the promontory may initiate long-term subsidence, when the ridge northern flank will have started withdrawing from beneath the promontory. On a shorter timescale, glacio-eustatic sea level changes have controlled the emergence and submergence of the promontory. During the last glacial stage, prior to ∼20 kyr, when the sea level was ∼120 m lower than today (Hacq *et al.* 1987), the 60–120 m deep Atacames Promontory was likely emerged, and consequently had no influence on tsunami wave propagation. Obviously, in light of this brief analysis, the geological evolution of the shelf promontory will not have a direct effect on tsunami hazard on a human timescale. We simply consider the tsunami signature of the Atacames promontory as it is nowadays.

3 THE SMFS AND EARTHQUAKES SCENARIOS

Ratzov *et al.* (2007) provided evidence for several areas of sediment instabilities characterized by remarkable SMFs scars. They are mainly located along the flanks of the submarine canyon and at the toe of the continental slope (Fig. 1). Our numerical tools are not adapted for the former SMFs because the SMF model component that estimates the initial wave, considers only uni-directional slides. Along the flanks of the canyon, where slid volumes are subject to multiple reorientations, it is tedious to reproduce these strong constraints. Consequently we chose two SMFs, S1 and S2 at the toe of the margin lower slope (see their positions and depths in Table 1), which are associated with clear mass transport deposits in the trench (Ratzov *et al.* 2010). These SMFs likely approximately slid within

Table 1. TOPICS input data are: estimate of the volume V of each identified submarine mass failure (SMF); the longitude and latitude of the SMF centroid (x_o, y_o), the supposed centre of mass; the centroid initial depth d (before the slides): it corresponds to the depth of the scar centre detected in the bathymetry minus half of the maximum thickness w; the length L (axis along the direction of slide) and width l (axis across the direction of slide); the mean azimuth (direction of slide) ϕ defined counter-clockwise and the mean slope θ along slide. TOPICS output are: the characteristic initial tsunami wavelength λ_c, the slide initial acceleration a_i, terminal velocity v_t and its characteristic duration t_c and the characteristic distance d_c. C_i and T_i represent the initial crest and trough amplitudes, respectively. Note that the SMF volumes are reconstructed as ellipsoids defined by $V = \pi L w l / 4$ to fit the numerical wavemaker model of Grilli & Watts (2005).

SMF	S1	S2
V (km³)	11.3	1.3
x_o (deg.)	80.257°W	80.254°W
y_o (deg.)	1.340°N	1.331°N
d (m)	3050	3090
L (m)	6418	2817
l (m)	9772	3882
w (m)	229	151
ϕ (deg.)	87	87
θ (deg.)	8	8
λ_c (m)	45908	30613
a_i (m s⁻²)	0.408	0.408
v_t (m s⁻¹)	108	72
t_c (s)	265	176
d_c (m)	28769	12627
C_i (m)	2.4	0.43
T_i (m)	−5.2	−0.58

a mean constant slope (Fig. 1). We reconstructed the slid SMFs and estimated the parameters required for calculating the initial tsunami wave (see Table 1 for details of the parameters). Because scar S2 is ensconced within S1, the two SMFs only differ in size in our models. Therefore, comparision between these two simulations allows for testing the sensitivity of the interplay between tsunami and promontory to wave heights.

During the twentieth century, the subduction of the Nazca plate beneath the Northern Ecuador/Southern Colombia margin generated four megathrust earthquakes in the last century: The $M_w = 8.8$ major event occurred in 1906 (see location in Fig. 1). it was followed by three important ones, that is, the $M_w = 7.8$ of 1942, the $M_w = 7.7$ of 1958 and the $M_w = 8.2$ of 1979 events (Fig. 1A) showing the segmentation and the successive reactivations of the area. Details on the morphology and the rupture processes of the area can be found in Collot *et al.* (2004). To perform our tsunami process study in the vicinity of the promontory we have selected the 1942 and the 1958 earthquake events because their subsequent potential tsunamis may display various directivities relative to the area. Without loss of generality, we took a similar earthquake magnitude for the two events (approx. $M_w = 7.84$) and we used the epicentre locations identified by Mendoza & Dewey (1984) (Table 2). The other rupture informations (in particular the dip angle and the focal depth) are derived from two seismic profiles (SIS44 and SIS22) gathered during the SISTEUR cruise operated onboard the R/V Nadir during autumn 2000: the profile SIS44 in the vicinity of the 1958 event (see Collot *et al.* 2004, for the profile) and the SIS-22 in the vicinity of the 1942 event (see d'Acremont *et al.* 2005, for the profile; see Fig. 1 for both track locations). Our purpose here is to try to extract robust conclusions on the tsunami signature. We want to check whether the spatial normalized wave height distribution at the coast is conserved or not, depending on the location of the tsunami source and the wave directivity.

Table 2. Okada's (1985) input parameters (first 10 lines) and outputs (last four lines) for two tsunami sources representative of the 1942 May 14 and 1958 January 19 earthquakes: longitude and latitude of segment centroid (x_o, y_o); the centroid depth d, the fault strike angle φ (clockwise from North); the fault rake angle λ (counter-clockwise from strike) which is taken here for a pure thrust ($90°$); the fault dip angle δ with the horizontal plane; the maximum fault slip Δ; the segment length along and width across (L, W); and the medium shear modulous μ; the seismic moment M_o; the derived magnitude M_w; the characteristic initial tsunami wavelength λ_o and period τ_o; and the characteristic tsunami trough and peak amplitudes η_o. Note that, in the simulation, slip is maximum at the segments' centroid and drops by 50 per cent at a radius of L from it.

Parameters	1942	1958
x_o	80.39°W	79.59°W
y_o	0.01°N	1.14°N
d (km)	12	18
φ	41°	71°
λ	90°	90°
δ	13°	11°
Δ (m)	6	6
L (km)	90	90
W (km)	30	30
μ (Pa)	4×10^{10}	4×10^{10}
M_o (J)	5.75×10^{20}	5.75×10^{20}
M_w	7.84	7.84
λ_o (km)	30	30
τ_o (s)	177	177
η_o (m)	-1.33; $+1.99$	-1.33; $+1.99$

© 2010 The Authors, *GJI*, **184**, 680–688
Geophysical Journal International © 2010 RAS

4 CONSTRUCTION OF THE NUMERICAL SIMULATION

Briefly, the numerical model used here is GEOWAVE which is composed of two numerical tools: TOPICS, that estimates the initial sea surface deformation due to the SMF (Grilli & Watts 1999) and FUNWAVE model that computes the tsunami propagation and inundation (Wei & Kirby 1995; Wei *et al.* 1995). As far as TOPICS is concerned, the initial free surface elevation and water velocities are derived from multivariate, semi-empirical curve fits as a function of non-dimensional parameters characterizing the landslide (e.g. density, geometry, location and slide orientation) and the local bathymetry (e.g. slope and mean depth). Relevant non-dimensional parameters were selected based on numerical experiments constrained by experiments that were carried out first with the 2-D model of (Grilli & Watts 1999). Then the curve fits were modified based on results from a more recent 3-D model (Grilli *et al.* 2002). The TOPICS-derived initial wave is transferred into FUNWAVE tsunami propagation and runup model. The model is fully non-linear and dispersive, retaining information to leading order in frequency dispersion $O[(kh)^2]$ and to all orders in non-linearity a/h (where k denotes an inverse wavelength scale, a denotes a wave amplitude and h denotes a water depth) (Wei & Kirby 1995; Wei *et al.* 1995). The model hosts a moving shoreline algorithm and includes bottom friction, energy dissipation to account for the wave breaking and a subgrid turbulence scheme (Chen *et al.* 2000; Kennedy *et al.* 2000). Although GEOWAVE has been validated for several SMFs (Watts *et al.* 2003; Ioualalen *et al.* 2010), the numerical simulation of the volume slide itself is not performed directly. The initial wave provided by TOPICS is an estimate only. Then its propagation can be considered fully reliable since FUNWAVE has already been validated for earthquake-derived tsunamis, for example, Ioualalen *et al.* (2007b). As a consequence, the simulated wave heights will not be considered based on their absolute values but as estimates or orders of amplitudes.

In this study, the computational domain extends from 81.5°W to 78.5°W in longitude and from 0.5°S to 2°N (Fig. 1). It contains the Atacames Promontory and the main coastal city Esmeraldas in its vicinity. It also contains the SMF area as well as an extended region eastwards to describe sufficiently the slides. Besides, the lateral boundaries of the domain have been also optimized such that no coastal reflection or bores are forgotten. The grid spacing is 200 m in both horizontal directions (1680 × 1400 nodes) and an optimum time step of 0.3 s has been taken to avoid any numerical instability. 2.22 hr of effective propagation has been simulated to report for the first crests everywhere in the domain.

The bathymetric data at the continental slope and the trench were obtained from Simrad EM12D multibeam data (150 m of spatial resolution) (Collot *et al.* 2005). On the shelf, available digitalized marine charts were used. Elsewhere, ETOPO-2 data have been used to complement the bathymetry field. The onland topography was derived from the USGS Shuttle Radar Topography Mission (SRTM) (90 m of spatial resolution).

5 NUMERICAL RESULTS AND DISCUSSION

We try here to extract and propose substantial results on the tsunami signature at the coastal area surrounding the Atacames promontory: How does it effect the wave amplification/attenuation? Does it contribute to any shielding independent of tsunami source? Does it balance other processes like wave divergence (attenuation) at the Es-
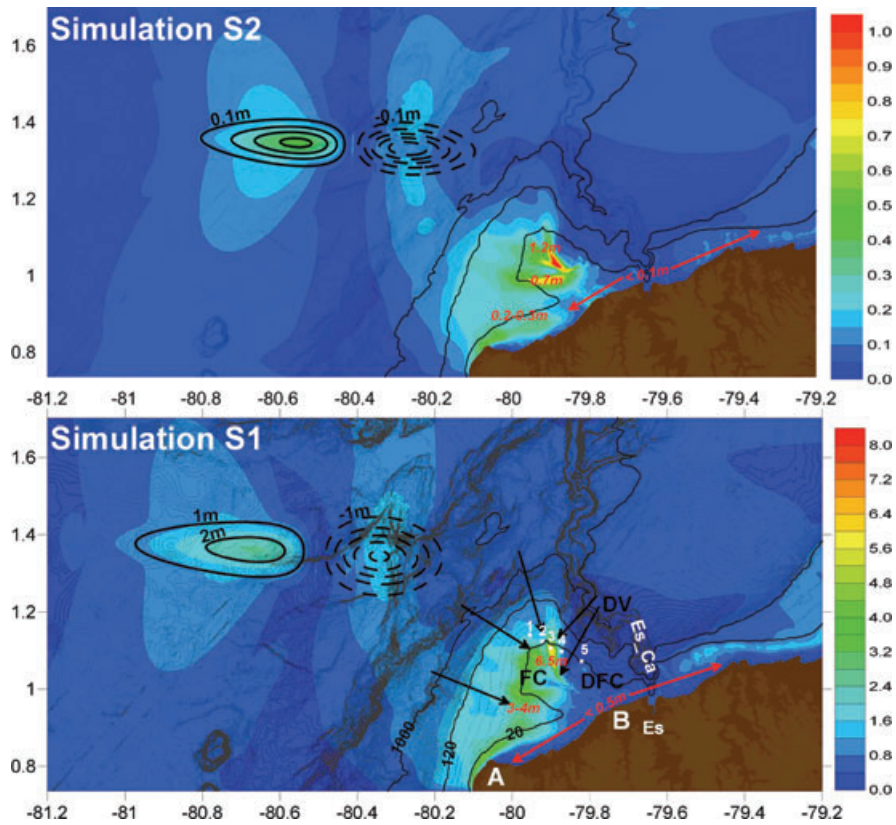
Figure 2. Initial surface elevation generated by TOPICS for SMFs S1 and S2 and their respective simulated maxima of elevation (colour map in metres). The highest waves are located (6.5 m for S1 and 1.2 m for S2). Dashed lines correspond to seafloor uplift (tsunami crest) and solid lines to subsidence (tsunami trough; 1 m and 0.1 m iso-contours for S1 and S2, respectively). The bathymetry is plotted in the background and isobathes 20, 120 and 1000 m are bolded. Es is for Esmeraldas, ES_Ca for Canyon of Esmeraldas. FC represents a focusing area while DFC stands for defocusing. DV is for a diverging wave propagation. Ascending white points 1–5 represent the wave directivity from the triggering source towards the coast (and towards the city of Esmeraldas).
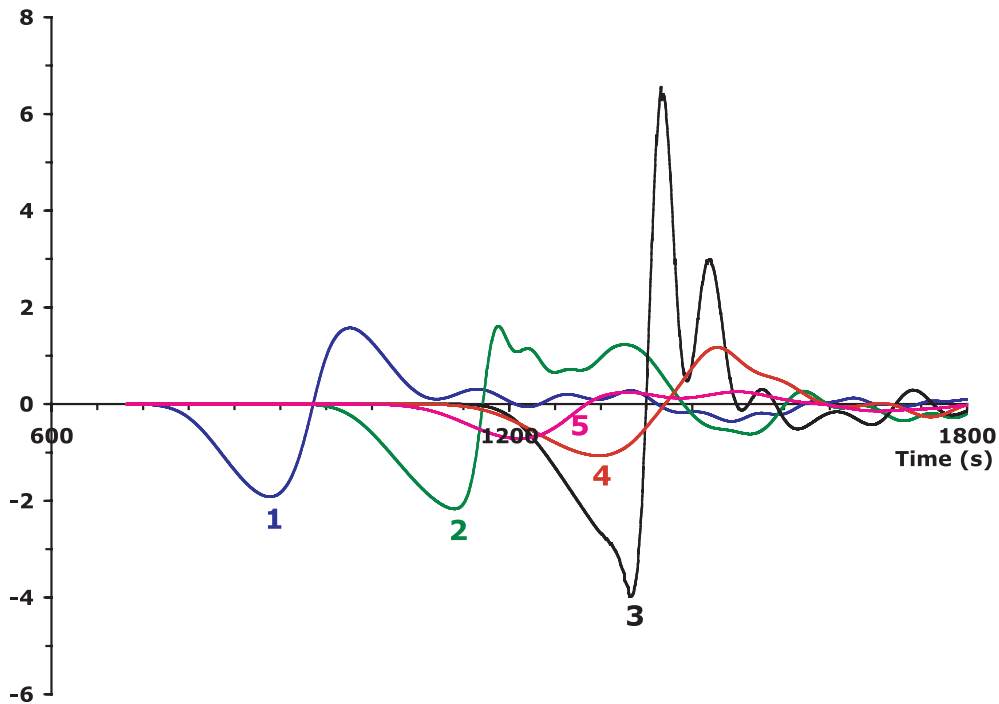

Figure 3. Wave height time-series (in metres) at the ascending white points 1–5 of Fig. 2. Time is in seconds ($t = 0$ being the time of slide S1 occurence).

meraldas submarine canyon termination. As far the SMFs-derived tsunamis are concerned, the wave trough is located in shallower water, for example, landward of the peak. For both simulations the maximum wave height (over the entire time of integration) occurs above the submerged platform (25–30 km offshore and not at the coast) with substantial waves for SMF S1 (Fig. 2). As stated above, we will consider in the following only orders of amplitudes. However, whatever the wave uncertainties are, the relative values (amplitudes relative to unity for the maximum wave) indicate that the tsunami risk, which is by definition at the coast, is negligible for the coastal area of the submerged promontory (from A to B in Fig. 2). This is an important issue: the presence of the submerged promontory acts as a natural protecting barrier. The reasons are easy to identify: first, shoaling (slope effect) acts mainly at the boarder of the promontory (at the 120 m isobath approx.) because the slope is relatively weak along the promontory. Then, the submerged promontory acts as a cape: the isobaths displayed in Fig. 2 indicate a concave-type shape (in particular the 120 m one). As a result, other modes of amplification/attenuation take the lead within the submerged promontory: for both SMFs, wave focusing areas are located offshore (FC in Fig. 2), then past the FC area, the wave defocuses (DFC in Fig. 2). The focusing process described here is identical for waves encountering conical islands and has been already detailed (Liu *et al.* 1995; Choi *et al.* 2007). The simulated synthetical tide gauges of Fig. 3 illustrate this process: along the wave propagation from points 1 to 5 (towards the coast and the city of Esmeraldas), the wave maxima is obtained at the point number 3 (6.5 m, offshore). Then the wave height decreases even with an operating shoaling with decreasing water depth.

In the vicinity of the promontory coastal area, the major city of Esmeraldas is only little impacted by the wave. Another factor that limits the wave impact on Esmeraldas is the concave-type shape of the isobaths within the Manglares Bay that forces a wave divergence. This is something usual aside capes: as an example, Ioualalen *et al.* (2010) showed for the French Riviera how the wave amplitude is enhanced by open bays surrounding the capes (at open bays, the wave diverges and escapes from its sides onto the capes). In their case, however, the capes were not submerged and they were effectively the location of maxima of wave amplitude. Another key feature is the presence of the Esmeraldas Canyon. The upward termination of the canyon, like most canyons, present concave-type isobaths that should provoke a wave divergence and place the maxima of amplitude aside the canyon termination where the city of Esmeraldas is located (Ioualalen *et al.* 2007a). A wave sequence is provided in Fig. 4: after 10 min of propagation, the wave encounters a refraction process at the Atacames Promontory due to the variable bathymetric field. Then, after 15 min the wave focuses at the Atacames Promontory and diverges at the Manglares Bay. After 20 min the wave reaches its maximum of amplitude at the focusing area. The defocused wave reaches Esmeraldas after 30 min of propagation.

The two earthquake scenarios of 1942 and 1958 with two distinct directivities yield substantial local tsunami heights (Fig. 5). This is particularly the case for the 1942 event because the earthquake has been located at deeper water (more shoaling effects). The maximal waves affect the whole Western coast while the northern coast is not impacted. There, local maximum wave height occurs offshore, above the Atacames promontory at approximately 79.8°W–1°N. The 1958 event was located in front of the Northern coast, therefore the coast is much more impacted than during the previous simulation. However, at the vicinity of the Atacames submerged promontory, the coast is less impacted, and as previously, local
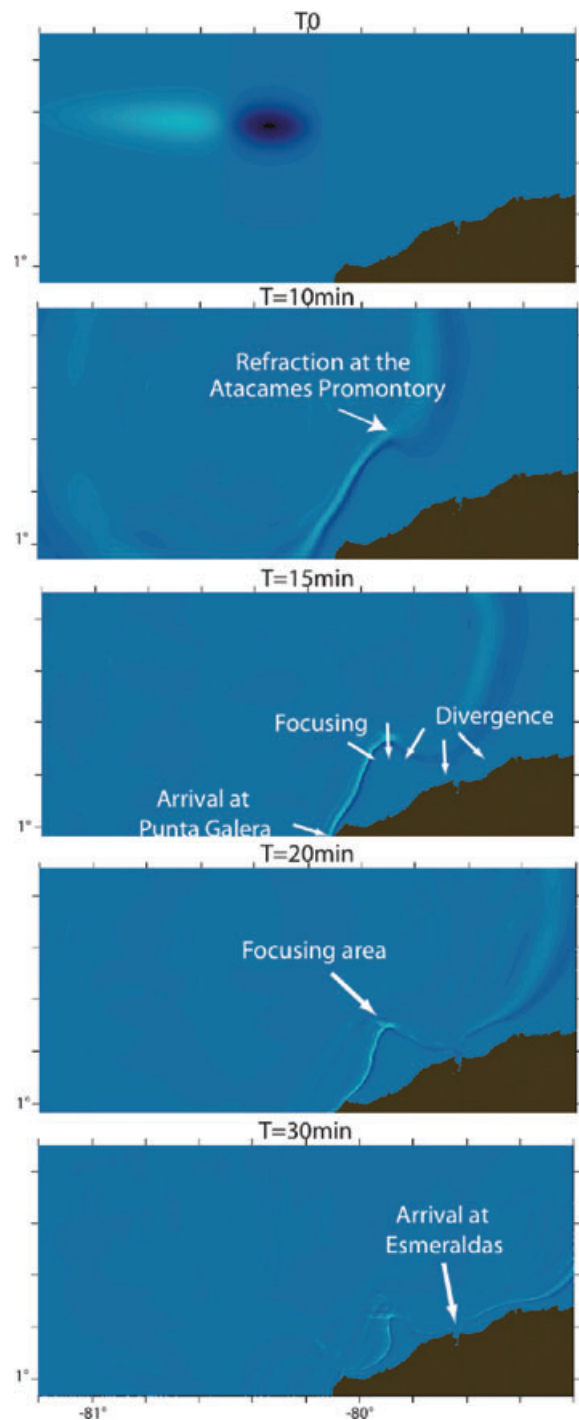
Figure 4. Wave propagation sequence at times *t*0 (initial wave formation), 10 min, 15 min, 20 min and 30 min. Dark blue represents a trough while light blue is for wave crest.

maximum wave height occurs offshore, above the promontory. Aside the coastal area of the promontory, the city of Esmeraldas is relatively sheltered (Fig. 5) for the same reasons as for the SMFs-derived tsunamis (wave divergence and canyon effect). This is in agreement with tsunami observations for the two historical events: the 1942 tsunami did not impact the city and the 1958 caused four victims but in the surrounding of the city only (see the simulated relatively high wave immediately west of the city in Fig. 5).
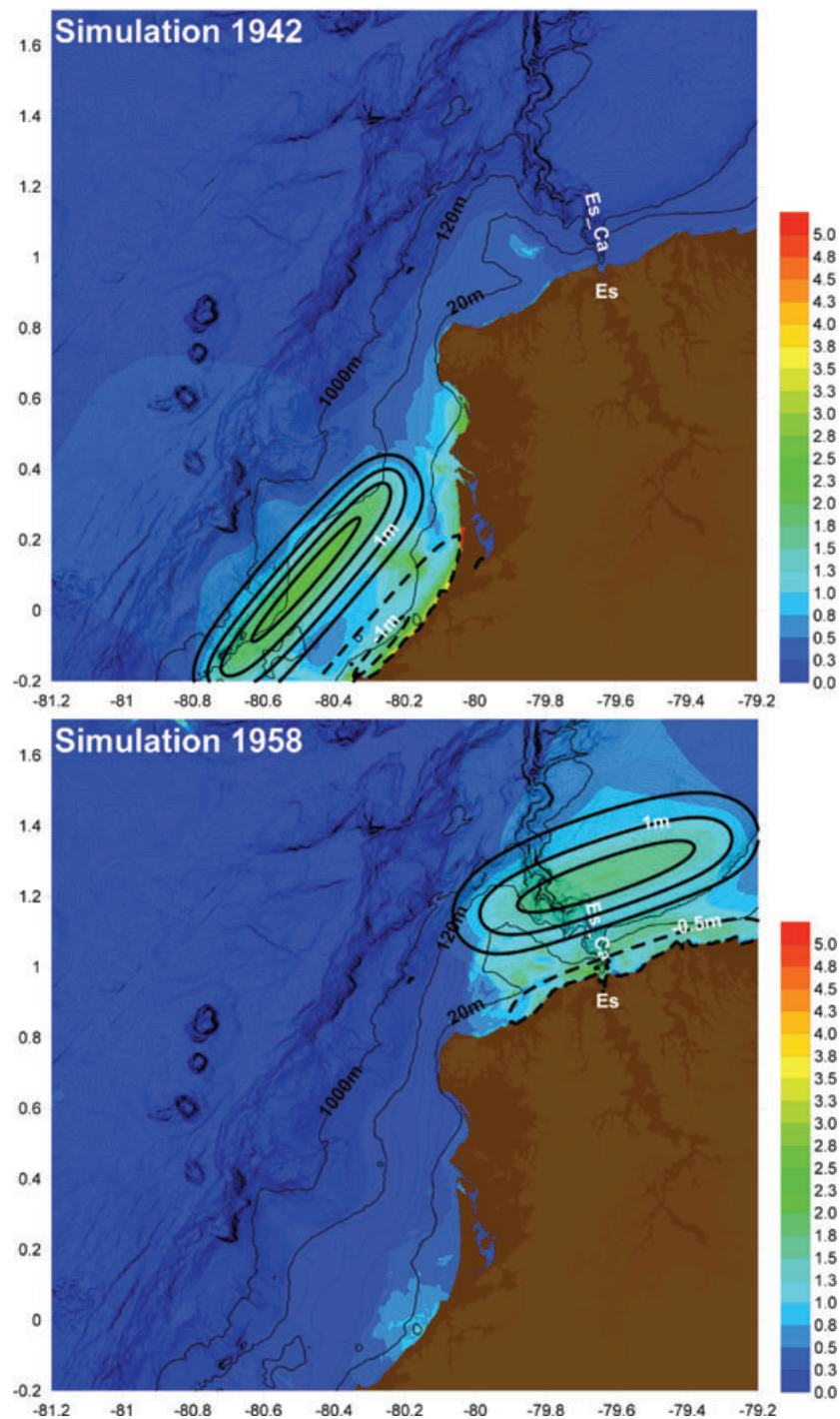
Figure 5. Same as Fig. 2 for the 1942 and 1958 earthquake-derived tsunamis. The initial surface elevation is computed with Okada (1985)'s dislocation model (0.5 m iso-contours). See Table 2 for the rupture parameters.

Moreover, the 1979 Colombia–Ecuador earthquake (located further north, Fig. 1) caused a tsunami that did not impact the city.

The numerical simulations proposed here are testing different wave directivities and amplitudes. Although they show a different wave distribution at the scale of the whole investigated Ecuadorian coast, the observations at the vicinity of the Atacames submerged promontory are quite similar. Regardless of the wave directivity and amplitudes, the concave shape of the seafloor generates wave focusing offshore, above the submerged promontory, thus locally naturally protecting the coast from the highest threat.

6 CONCLUSIONS

This work concerns the tsunami signature at a submerged (marine) promontory. For that purpose, we have considered the case study of the Atacames Promontory, Ecuador. To assess a robust particular signature, we have considered a representative set of tsunami sources: Based on the local bathymetry we have identified two ancient SMF scars close to each other that differ significantly in size. In complement, we have constructed two earthquake sources representative of the 1942 May 14 and the 1958 January 19 events that

have been located in the vicinity of the promontory. These two latter sources are of similar magnitude but differ significantly in position and orientation (yielding different tsunami wave directivity). We found out that the submerged promontory acts as a cape displaying a concave-type shape yielding a strong wave refraction process. This process induces a wave focusing area offshore. Then the wave defocuses before reaching the coast. As a result, the promontory is acting as a local tsunami shielding process.

These processes can be considered as generic for any submerged promontory. As an example, the shelf of the Nile Delta, Egypt, also exhibits a concave-shape bathymetry: Garziglia *et al.* (2007) also identified ancient substantial landslide scars and their tsunami simulations also indicate a focusing/defocusing process at the shelf which shelters the Nile Delta area from a tsunami threat contrary to Alexandria city. The effect of natural protection due to the bathymetry shape has been shown also for the Korean coast using a shallow water model along with ray theory equations (Choi *et al.* 2005): here we showed such natural behaviour through numerical experiments for our case study. The choice of realistic SMFs and earthquakes and the variety of the derived tsunami directivities confirm the robustness of the results. Besides, for that particular case study, the tsunami risk for the major city of Esmeraldas is not strictly affected by the presence of the promontory because it is not in its coastal zone of influence. The tsunami signature for this city is rather due to the wave limiting impact of the canyon and the divergent waves: we have considered its tsunami signature because it was in our computational domain.

ACKNOWLEDGMENTS

REFERENCES

Assier-Rzadkiewicz, S., Heinrich, P., Sabatier, P.C., Savoye, B. & Bourillet, J.F., 2000. Numerical modelling of a landslide-generated tsunami : the 1979 Nice event, *Pure appl. Geophys.,* **157,** 1707–1727.

Beck, S.L. & Ruff, L.J., 1984. The rupture process of the great 1979 Colombia earthquake: evidence for the asperity model, *J. geophys. Res.,* **89,** 9281–9291.

Chen, Q., Kirby, J.T., Dalrymple, R.A., Kennedy, A.B. & Chawla, A., 2000. Boussinesq modeling of wave transformation, breaking, and run-up. II: 2D, *J. Waterway, Port, Coastal, Ocean Eng.,* **126,** 48–56.

Choi, B.H., Pelinovsky, E., Lee, H.J. & Woo, S.B., 2005. Estimates of tsunami risk zones on the coasts adjacent to the East (Japan) Sea based on the synthetic catalogue, *Nat. Hazards,* **36**(2), 355–381.

Choi, B.H., Kim, D.C., Pelinovsky, E. & Woo, S.B., 2007. Three-dimensional simulation of tsunami run-up around conical island, *Coastal Eng.,* **8,** 618–629.

Collot, J.-Y. *et al.,* 2004. Are rupture zone limits of great subduction earthquakes controlled by upper plate structures? Evidence from multichannel seismic reflection data acquired across the northern Ecuador-southwest Colombia margin, *J. geophys. Res.,* **109,** B11103, doi:10.1029/2004.JB003060.

Collot, J.-Y., Michaud, F., Legonidec, Y., Calahorrano, A., Sage, F., Alvarado, A. & el personal cientifico y tecnico del INOCAR, 2005. Mapas del margen continental centro y sur de Ecuador : Batimetria, relieve, reflectividad acustica e interpretacion geologica, *Publicacion IOA - CVM - 04 - POST.*

Collot, J.-Y. *et al.,* 2010. Vision general de la morfologa submarina del margen convergente de Ecuador-Sur de Colombia: implicaciones sobre la transferencia de masa y la edad de la subduccion de la Cordillera de Carnegie, in *Sintesis de los Resultados de Investigacion Geologica y Geofisica Sobre el Margen Ecuatoriano, la Costa, la Cordillera Submarina de Carnegie, y de la Plataforma Volcanica de Galapagos,* eds Collot, J.-Y., Sallares, V. & Pazmio, A., pp. 47–74, Publicacion CNDM-INOCAR-IRD, PSE001-09, Guayaquil, Ecuador.

D'Acremont, E., Ribodetti, A., Collot, J.-Y. & Sage, F., 2005. Margin structure and destabilisation processes on the Colombia-Ecuador margin by 2D quantitative seismic imaging, *General Assembly EGU,* Vienna, Austria, 2005 April 24–29.

Garziglia, S., Ioualalen, M., Migeon, S., Ducassou, E., Sardoux, O., Brosolo, L. & Mascle, J., 2007. Triggering factors and tsunamigenic potential of a large submarine mass failure on the Western Nile Margin (Rosetta Area, Egypt), in *Submarine Mass Movements and Their Consequences,* pp. 347–356, eds Lykousis, V., Sakellariou, D. & Locat, J., Springer, Dordrecht.

Grilli, S.T. & Watts, P., 1999. Modeling of waves generated by a moving submerged body: Applications to underwater landslides, *Eng. Analysis with Boundary Elements,* **23**(8), 645–656.

Grilli, S.T. & Watts, P., 2005. Tsunami generation by submarine mass failure Part I: Modeling, experimental validation, and sensitivity analysis, *J. Waterway, Port, Coastal and Ocean Eng.,* **131**(6), 283–297.

Grilli, S.T., Vogelmann, S. & Watts, P., 2002. Development of a 3D numerical wave tank for modeling tsunami generation by underwater landslides, *Eng. Analysis with Boundary Elements,* **26**(4), 301–313.

Hacq, B.U., Hardenbol, J. & Vail, P.R., 1987. Chronology of fluctuating sea levels since the Triassic, *Science,* **235,** 1156–1167.

Ioualalen, M., Pelinovsky, E., Asavanant, J., Lipikorn, R. & Deschamps, A., 2007a. On the weak impact of the 26 December Indian Ocean tsunami on the Bangladesh coast, *Nat. Hazards Earth Sys. Sci.,* **7,** 141–147.

Ioualalen, M., Asavanant, J., Kaewbanjak, N., Grilli, S.T., Kirby, J.T. & Watts, P., 2007b. Modeling the 26th December 2004 Indian Ocean tsunami: case study of impact in Thailand, *J. geophys. Res.,* **112,** C07024, doi:10.1029/2006JC003850.

Ioualalen, M., Migeon, S. & Sardou, O., 2010. Landslide tsunami vulnerability in the Ligurian Sea: case study of the 1979 Nice airport submarine landslide and of identified geological mass failure, *Geophys. J. Int.,* **181,** 724–740, doi:10.1111/j.1365-246X.2010.04572.x.

Kanamori, H. & McNally, K.C., 1982. Variable rupture mode of the subduction zone along the Ecuador-Colombia coast, *Bull. seism. Soc. Am.,* **72**(4), 1241–1253.

Kennedy, A.B., Chen, Q., Kirby, J.T. & Dalrymple, R.A., 2000. Boussinesq modeling of wave transformation, breaking, and run-up. I: 1D, *J. Waterway, Port, Coastal, Ocean Eng.,* **126,** 39–47.

Liu, P.L.B., Cho, Y.S., Briggs, M.J., Kanoglu, U. & Synolakis, C.E., 1995. Run-up of solitary wave on a circular island, *J. Fluid Mech.,* **302,** 259–285.

Mendoza, C. & Dewey, J.W., 1984. Seismicity associated with the great Colombia–Ecuador earthquakes of 1942, 1958 and 1979: implications for barrier models of earthquake rupture *Bull. seism. Soc. Am.,* **74**(2), 577–593.

Michaud, F., J.-Y. Collot, A., Alvarado, Lopez, E. & the technical staff of INOCAR, 2006. Repblica del Ecuador, Batimetra y Relieve Continental e insular, *Publicacion IOA-CVM-01-Post,* INOCAR, Guayaquil, Ecuador.

Okada, Y., 1985. Surface deformation due to shear and tensile faults in a half-space, *Bull. seism. Soc. Am.,* **75**(4), 1135–1154.

Pedoja, K. *et al.,* 2006. Plio-Quaternary uplift of the Manta Peninsula and La Plata Island and the subduction of the Carnegie Ridge, central coast of Ecuador, *J. South Am. Earth Sci.,* **22**(1–2), 1–21.

Ratzov, G., Sosson, M., Collot, J.-Y., Migeon, S., Michaud, F., Lopez, E. & Le Gonidec Y., 2007. Submarine landslides along the North Ecuador South Colombia convergent margin: possible tectonic control, in *Submarine Mass Movements and Their Consequences,* pp. 47–55, eds Lykousis, V., Sakellariou, D. & Locat, J., Springer, Dordrecht.

Ratzov, G., Collot, J.-Y., Sosson, M. & Migeon, S., 2010. Mass transport deposits in the northern Ecuador subduction trench: result from frontal erosion over multiple seismic cycles, *Earth planet. Sci. Lett.,* **296,** 89–102.

Smith, W.H.F. & Sandwell, D.T., 1997. Global seafloor topography from satellite altimetry and ship depth soundings, *Science,* **277,** 1957–1962.

Tappin, D.R., Watts, P. & Grilli, S.T., 2008. The Papua New Guinea tsunami of 17 July 1998: anatomy of a catastrophic event, *Nat. Hazards Earth Syst. Sci.,* **8,** 243–266.

Trenkamp, R., Kellogg, J.N., Freymueller, J.T. & Mora, P., 2002. Wide plate margin deformation, southern Central America and northwestern South America, CASA GPS observations, *J. South Am. Earth Sci.,* **15**(2), 157–171.

Watts, P., Grilli, S.T., Kirby, J.T., Fryer, G.J. & Tappin, D.R., 2003. Landslide tsunami case studies using a Boussinesq model and a fully nonlinear tsunami generation model, *Nat. Hazards and Earth Sci. Systems,* **3**(5), 391–402.

Wei, G. & Kirby, J.T., 1995. A time-dependent numerical code for extended Boussinesq equations, *J. Waterway, Port, Coastal, Ocean Eng.,* **121,** 251–261.

Wei, G., Kirby, J.T., Grilli, S.T. & Subramanya, R., 1995. A fully nonlinear Boussinesq model for free surface waves. Part 1: highly nonlinear unsteady waves, *J. Fluid Mech.,* **294,** 71–92.